RESEARCH ARTICLE
ATMOSPHERIC PHYSICS

Earth and Planetary Physics
2: 40–51, 2018
doi: 10.26464/epp2018004

Accuracy of radar-based precipitation measurement: An analysis of the influence of multiple scattering and non-spherical particle shape

Hao Chen[1,2], JinHu Wang[1,3,4*], Ming Wei[1,2], and HongBin Chen[4]

[1]Collaborative Innovation Center on Forecast and Evaluation of Meteorological Disasters, Key Laboratory for Aerosol-Cloud-Precipitation of China Meteorological Administration, Nanjing University of Information Science and Technology, Nanjing 210044, China;

[2]State Key Laboratory of Severe Weather, Chinese Academy of Meteorological Sciences, Beijing 100081, China;

[3]National Demonstration Center for Experimental Atmospheric Science and Environmental Meteorology Education, Nanjing University of Information Science & Technology, Nanjing 210044, China;

[4]Key Laboratory of Middle Atmosphere and Global Environment Observation, Institute of Atmospheric Physics, Chinese Academy of Sciences, Beijing 100029, China

Abstract: Two assumptions are typically made when radar echo signals from precipitation are analyzed to determine the micro-physical parameters of raindrops: (1) the raindrops are assumed to be spherical; (2) multiple scattering effects are ignored. Radar cross sections (RCS) are usually calculated using Rayleigh's scattering equation with the simple addition method in the radar meteorological equation. We investigate the extent to which consideration of the effects of multiple scattering and of the non-spherical shapes within actual raindrop swarms would result in RCS values significantly different from those obtained by conventional analytical methods. First, we establish spherical and non-spherical raindrop models, with Gamma, JD, JT, and MP size distributions, respectively. We then use XFDTD software to calculate the radar cross sections of the above raindrop models at the S, C, X and Ku radar bands. Our XFDTD results are then compared to RCS values calculated by the Rayleigh approximation with simple addition methods. We find that: (1) RCS values calculated using multiple scattering XFDTD software differ significantly from those calculated by the simple addition method at the same band for the same model. In particular, for the spherical raindrop models, the relative differences in RCS values between the methods range from a maximum of 89.649% to a minimum of 43.701%; for the non-spherical raindrop models, the relative differences range from a maximum of 85.868% to a minimum of 11.875%. (2) Our multiple scattering XFDTD results, compared to those obtained from the Rayleigh formula, again differ at all four size distributions, by relative errors of 169.522%, 37.176%, 216.455%, and 63.428%, respectively. When nonspherical effects are considered, differences in RCS values between our XFDTD calculations and Rayleigh calculations are smaller; at the above four size distributions the relative errors are 0.213%, 0.171%, 7.683%, and 44.514%, respectively. RCS values computed by considering multiple scattering and non-spherical particle shapes are larger than Rayleigh RCS results, at all of the above four size distributions; the relative errors between the two methods are 220.673%, 129.320%, 387.240%, and 186.613%, respectively. After changing the arrangement of particles at four size distributions in the case of multiple scattering effect and non-spherical effect, the RCS values of Arrangement 2 are smaller than those of Arrangement 1; the relative errors for Arrangement 2, compared to Rayleigh, are 60.558%, 76.263%, 85.941%, 64.852%, respectively. We have demonstrated that multiple scattering, non-spherical particle shapes, and the arrangement within particle swarms all affect the calculation of RCS values. The largest influence appears to be that of the multiple scattering effect. Consideration of particle shapes appears to have the least influence on computed RCS values. We conclude that multiple scattering effects must be considered in practical meteorological detection.

Keywords: Finite difference time domain (FDTD); generalized Lorenz Mie theory; raindrops; RCS; multiple scattering; oblate ellipsoid particle

Citation: Chen, H., Wang, J. H., Wei, M., and Chen, H. B. (2018). Accuracy of radar-based precipitation measurement: An analysis of the influence of multiple scattering and non-spherical particle shape. *Earth Planet. Phys.*, *2*, 40–51. http://doi.org/10.26464/epp2018004

1. Introduction

The quantitative measurement of precipitation by conventional radar plays a very important role in the weather forecasting, especially in flood disaster prediction (Chen MX et al., 2004; Wang GL et al., 2007). Radar electromagnetic waves propagating in the atmosphere are scattered and absorbed by clouds and precipitation (Li SH et al., 2014; Wang JH et al., 2013, 2016a; Wu JX et al., 2012), which not only greatly affects the remote sensing performance of conventional radar, but also affects the retrieval accuracy

Correspondence to: J. H. Wang, goldtigerwang@nuist.edu.cn
Received 13 SEP 2017; Accepted 19 DEC 2017.
Accepted article online 19 JAN 2018.

of microphysical parameters. Therefore, investigation of scattering characteristics of raindrops at the centimeter band is very important for improving the accuracy of atmospheric detection, climate sensing, and other fields.

The scattering characteristics of precipitation particles are related to phase, size, shape and other parameters (Mason, 1979). In theoretical models, hydrometeors are usually simplified into spherical particles; small raindrops can indeed be approximately spherical, but large raindrops should usually be regarded as approximately ellipsoid or flat bottomed ellipsoid, due to surface tension (Liu XC et al., 2013). In order to better understand the scattering effect of raindrops and to more accurately retrieve the microphysical parameters of precipitation, the relationship between the electromagnetic waves emitted by meteorological radar and actual raindrop shapes should be solved.

At present, the algorithms for calculating the scattering of raindrops are FDTD (finite difference time domain) (Yang P and Liou, 1996), DDA (discrete dipole approximation) (Draine and Flatau, 1994), T-matrix (Mishchenko et al., 1996), FEM (finite element method) (Baia et al., 2017), Mom (method of moments) (Wang K et al., 2017), GOM (geometric optical method) (Konoshonkin et al., 2016), PSTD (pseudo-spectral time domain method) (Liu C et al., 2012a, b) and ADT (anomalous diffraction theory) (Loiko et al., 2017) etc.

Atlas et al. (1953) used Gans theory to calculate scattering and attenuation of radar by small rotational ellipsoids, and have given the expression for small ellipsoid scattering. Seliga and Bringi (1978) studied the differential scattering properties of classes of hydrometeors at linear orthogonal polarizations using Waterman's T-matrix mehod. Also, Liu LP and Xu BX (1991) used the T-matrix method to study how 5.6 cm radar waves at different phases are scattered and attenuated by hail. Wang ZH (2002, 2003) and Xu XY (2002) conducted experimental measurements of scattering by flat ellipsoids non-spherical shapes characteristic of rain and hail and compared their results with those calculated by DDA; Studies of the effects of non-spherical raindrops in radar detection, however, are not sufficient. Raindrops have a certain size and shape distribution that must be taken into consideration. Eremin et al. (1995) used the discrete source method to study the multiple scattering of raindrops under linear permutation conditions.

At present, the multiple scattering characteristics of lidar echoes have been extensively studied (Kunkel and Weinman, 1976; Mooradian et al., 1980; Spinhirne, 1982). Platt and Dilley (1984) argued that multiple scattering varies with the optical thickness, extinction of clouds, and depth of Lidar penetration; Bruscaglioni et al. (1995) studied multiple scattering effects by analyzing satellite laser technology; Li YY et al. (2008) used the semi-analytic Monte Carlo method to simulate the echo signal of multiple scattering lidars; their results showed that the influence of multiple scattering on cirrus was obvious; Xiong XL et al. (2014) proposed a new method for solving the lidar ratio in Mie scattering lidar, considering the influence of multiple scattering.

Compared with lidar, little research has been done to determine multiple scattering effects of raindrops on centimeter-wavelength radar, which is an important means of precipitation detection (Zhong et al., 2009; Wang JH et al., 2014, 2016b, c). Therefore, the objective of this paper is to study multiple scattering effects of non-spherical raindrops in a certain size distribution, when subjected to conventional centimeter-wavelength radar. We base our analysis on the FDTD algorithm and compare our results with those from the simple addition method. We thus provide a theoretical basis for improving the accuracy of characteristics of precipitation particle swarms, based on conventional centimeter-wavelength radar data.

2. Attributes of Raindrops

2.1 Shapes of Raindrops

The shapes of falling raindrops are usually affected by gravity, buoyancy, and drag forces. A semi-empirical physics model (Pruppacher and Pitter, 1971) shows: when their equivalent radius $r\leq$ 0.017 cm, raindrops can be approximated as small spheres; when 0.017 cm$<r<$0.05 cm, raindrops can be treated as oblate ellipsoids; when $r\geq$0.05 cm, raindrops tend to be flat oblate ellipsoids.

In theoretical research, the shape of all raindrops is usually approximated as oblate ellipsoid, which can be found in Figure 1.

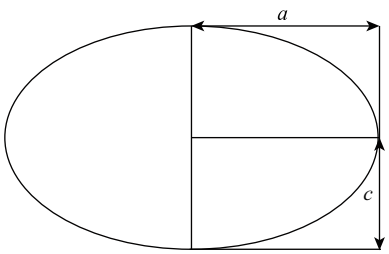

Figure 1. The rotating oblate ellipsoid.

The relationship between the axial ratio of the oblate ellipsoid and the spherical equivalent diameter of raindrops tested by Pruppacher and Beard (1970) in wind tunnel studies can be found below equation (1). Their investigations were carried out by means of a wind tunnel constructed at the University of California, Los Angeles (UCLA) for cloud physics research. Briefly, the tunnel, fabricated of aluminium and stainless steel, consists of a horizontal air conditioning system and a vertical flow control system. The air is propelled through these two systems by means of a vacuum pump. The air conditioning system allows the relative humidity of the tunnel air in the observation section to be varied in a controlled manner between 1 percent and 100 percent, and the temperature between room temperature and –40 °C. Their investigations identified three average raindrop shapes as raindrop volume increases:

$$\frac{c}{a}=\begin{cases}1.0, & 0<D_{\rm e}\leq 0.028\ {\rm cm}\\ \left[1-\left(\dfrac{9}{32}\right)\dfrac{D_{\rm e}\rho V_{\rm t}^2}{\mu}\right]^{0.5}, & 0.028<D_{\rm e}\leq 0.100\ {\rm cm}\\ 1.03-0.62D_{\rm e}, & 0.100<D_{\rm e}\leq 1\ {\rm cm}\end{cases}\quad(1)$$

where c is the radius of the axis of the rotating oblate ellipsoid, and its direction is vertical upward; a is the radius of the symmetry axis; $D_{\rm e}$ is the equivalent sphere diameter of the raindrop;

the saturated water vapor density is given by ρ=1.1937×10^{-3}g·cm^{-3}; the coefficient of surface tension of water is μ=72.75 erg·cm^{-3}; and V_t is the terminal velocity of free-falling raindrops (Liu XC et al., 2010; Atlas et al., 1973).

The power index raindrop velocity model used in the past is applicable only to raindrops with diameters less than 0.04 mm and cannot be used extensively. The more accurate estimation of terminal velocities in a swarm of free-falling raindrops at standard atmospheric pressure, put forward by Atlas et al. (1973), is as follows:

$$V_t = \begin{cases} 0, & D_e \leqslant 0.028\ \text{mm} \\ 4.323(D_e - 0.03), & 0.028\ \text{mm} < D_e < 0.6\ \text{mm} \\ 9.65 - 10.3e^{-0.6D_e}, & D_e \geqslant 0.6\ \text{mm} \end{cases} \quad (2)$$

2.2 Size Distributions of Raindrops

The change of raindrop concentration (the number of raindrops in a unit volume) with scale is called the raindrop size distribution $N(D)$, which represents the corresponding relation between the size D and the quantity N. N is a microphysical parameter that reflects the characteristics of ensembles of particles. The size distribution of actual precipitation is complicated and varies with the region, precipitation, cloud type, and the state of the underlying surface.

In order to compare the difference between the RCS computed by considering multiple scattering effects and the results of simple addition, the normalized functions of Gamma size distribution, JD (drizzle) size distribution, JT (rainstorm) size distribution, and MP size distribution were selected in this literature (Mätzler, 2002). The universal function of the four size distributions is

$$N(D) = N_0 D^{\mu} e^{-\lambda D}, \quad (3)$$

where D (unit: mm) is the equivalent diameter of particles, N_0 and λ are concentration and scale parameters, respectively, μ is the shape factor, N_0 is 8000 (unit: m^3·mm^{-1}), and R (unit: mm·h^{-1}) is precipitation intensity, R=10 mm/h.

The normalized size distribution function parameters are shown in Table 1.

2.3 Complex Refractive Index of Raindrops

For pure water, the empirical formulas of dielectric constant ε, temperature T, and wavelength λ can be found as follows (Zhang PC and Wang ZH, 1995):

$$\varepsilon = 4.9 + \frac{\varepsilon_s - 4.9}{1 + \frac{i\lambda_s}{\lambda}}, \quad (4)$$

$$\varepsilon_s = 88.2 - 0.40885t + 0.00081t^2, \quad (5)$$

$$\lambda_s = 1.8735116 - 0.027296t + 0.000136t^2 + 1.4662\exp(-0.0634t), \quad (6)$$

where λ (unit: cm) is the electromagnetic wavelength, t(unit: ℃), (–40<t<70, 1 ℃=273.15+K) is the temperature, 0 K of t, 10.7 cm (S), 5.6 cm (C), 3.2 cm (X) and 2.2 cm (Ku) of λ are selected in this paper. According to equations (4), (5), (6), the complex dielectric constant and complex refractive index of pure water precipitation particles at S, C, X and Ku bands are given in Table 2.

3. The Multiple Scattering Computation Methods of Raindrops

3.1 Finite Difference Time Domain

XFDTD is a full wave 3D electromagnetic field simulation software based on the finite difference time domain (FDTD) method. FDTD was developed by Yee (1996). In recent years, this method has been widely used to solve the interaction of various targets (including ice particles) and electromagnetic waves (Mishchenko, 1993; Mishchenko et al., 2000; Taflove, 1998; Taflove et al., 2000). FDTD uses the solution of time domain Maxwell's equations of rotation to calculate the scattering properties of particles. The remarkable advantage of FDTD is that the concept is simple and easy to implement, and the singular kernel problem of integral equation is avoided. Therefore, FDTD is more suitable for solving light scattering of complex shapes and inhomogeneous small particles (Xu LS et al., 2014).

Table 1. Parameters of normalized size distribution function

Size distribution	N_0 (R)/mm^{-4}	(Norm(R, P_0); X=ln(R))/mm	λ(R)/mm^{-1}	μ
Gamma	1.98×10^{-5}$R^{-0.384}$×Norm	1.047–0.0436X+0.0073X^2	5.38$R^{-0.186}$	2.93
MP	0.80×10^{-5}×Norm	0.842–0.00915X+0.0072X^2	2.00$R^{-0.21}$	0
JD	3.00×10^{-5}×Norm	1.1194–0.0367X+0.0079X^2	3.00$R^{-0.21}$	0
JT	0.14×10^{-5}×Norm	1.0945–0.0052X+0.0124X^2	1.00$R^{-0.21}$	0

Table 2. Complex dielectric constant and complex refractive index of precipitation particles at S, C, X and Ku bands

Bands	λ(cm)	Complex dielectric constant ε	Complex refractive index m
S	10.7	80.8053–23.6917i	9.0833–1.3044i
C	5.6	66.3458–36.6449i	8.4303–2.1734i
X	3.2	44.7712–41.6120i	7.2765–2.8594i
Ku	2.2	30.1082–38.2674i	6.2769–3.0483i

Using XFDTD to calculate the scattering process of precipitation particles is represented in a flow chart shown in Figure 2.

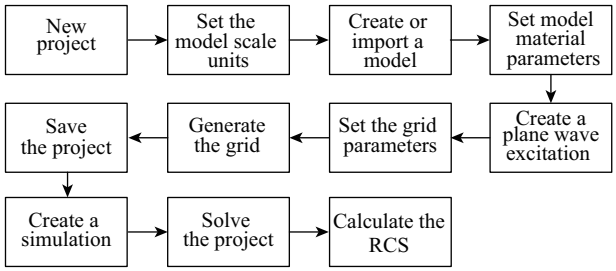

Figure 2. Calculation of RCS of precipitation particles by XFDTD.

3.2 Generalized Lorenz Mie Theory

The generalized multiple particle Mie theory (GMM) is a classical method for analyzing arbitrary swarms of spherical particles. The particles in a particle swarm are assumed to be isotropic and uniform but can be of different sizes and components (Xu YL, 1995; Xu YL and Gustafson, 1997). The GMM algorithm written by Yu-lin Xu for the scattering of particles (Mishchenko, 1993; Mishchenko et al., 2000) is a popular Fortran code. The code contains two input files, namely "gmm01f.par" and "gmm01f.in".The output file mainly contains the amplitude scattering matrix, the RCS of the total and differential scattering cross section, and the scattering intensity. The general calculation flow of the GMM algorithm is shown in Figure 3.

3.3 RCS Comparison Between Single Scattering and Multiple Scattering of Spherical Raindrops

Since the particles in the actual atmosphere are in the form of ensembles of particles of various sizes, it is necessary to study the multiple scattering problems of particle swarms. The raindrop models satisfying equation (3) and the four normalized raindrop size distribution functions shown in Table 1 were established, respectively. The number of particles in raindrop swarms were 18 in Gamma size distribution, 18 in JD size distribution, 17 in JT size distribution, and 17 in MP size distribution. The concrete parameters of raindrops are shown in Table 3.

The raindrop particles were arranged from large to small and located from bottom layer to top layer, and were divided into three layers except the Gamma size distribution. The diameters of the lowest layer of raindrops ranged between 3000 μm and 9000 μm; of the raindrops in the middle layer, the diameter range was 300 μm to 900 μm; the uppermost raindrops were assigned diameters between 100 μm and 250 μm. The distance between two adjacent raindrops in the same layer was chosen to be the sum of the diameters of the two raindrops; the vertical distance between adjacent layers was chosen to be the sum of the largest particle diameters in the two layers. The simulated raindrop models of XFDTD are presented in Figure 4.

The XFDTD software was used to calculate the RCS of the spherical raindrops as presented in Figure 4. XFDTD results were compared with the results obtained from the GMM algorithm and the simple addition method, tabulated in Table 4.

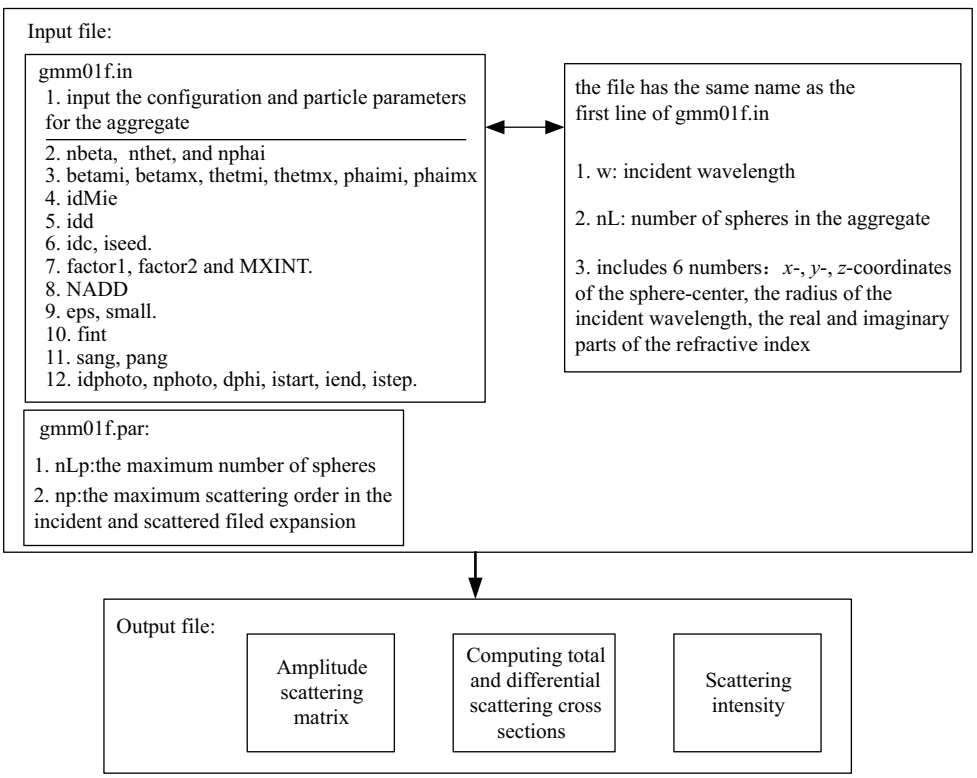

Figure 3. Flow of GMM algorithm for the calculation of scattering characteristics of a particle swarm.

Table 3. Size and size distribution of raindrops

Gamma size distribution												
Diameter(μm)	100	150	200	250	300	500	700	900	3000	5000	7000	9000
Number	0	0	0	0	1	2	2	2	2	2	2	2
JD size distribution												
Diameter(μm)	100	150	200	250	300	500	700	900	3000	5000	7000	9000
Number	1	2	2	2	2	2	2	2	0	1	1	1
JT size distribution												
Diameter(μm)	100	150	200	250	300	500	700	900	3000	5000	7000	9000
Number	0	1	1	1	1	1	1	2	2	2	2	3
MP size distribution												
Diameter(μm)	100	150	200	250	300	500	700	900	3000	5000	7000	9000
Number	1	1	1	2	1	2	2	2	1	1	1	2

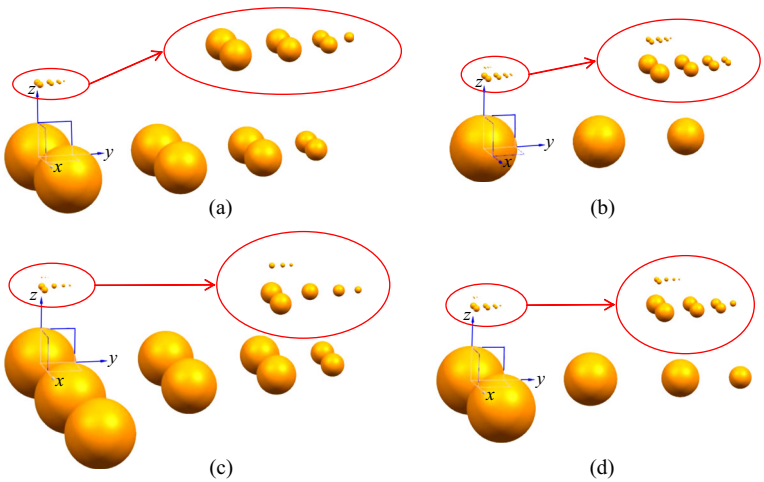

Figure 4. Spherical raindrop in the XFDTD software layout diagram. (a–d) Spherical raindrop arrangement in Gamma, JD, JT, and MP size distribution, respectively.

Table 4. Spherical raindrops RCS, comparing XFDTD, GMM, and the simple addition method (unit: dBm^2)

Size distribution	Method	S	C	X	Ku
Gamma	GMM	−50.950	−35.299	−27.500	−24.663
	XFDTD	−49.383	−35.009	−28.121	−24.532
	Simple addition method	−57.591	−40.980	−33.654	−33.496
JD	GMM	−55.777	−41.118	−33.474	−31.728
	XFDTD	−58.114	−38.132	−34.042	−30.858
	Simple addition method	−60.609	−43.992	−36.668	−36.532
JT	GMM	−47.174	−32.967	−25.418	−22.819
	XFDTD	−48.784	−29.819	−25.906	−22.812
	Simple addition method	−56.217	−39.507	−32.320	−32.662
MP	GMM	−51.502	−36.973	−29.465	−28.022
	XFDTD	−53.651	−33.909	−30.826	−27.691
	Simple addition method	−58.186	−41.419	−34.311	−34.973

Table 4 shows that the RCS values of spherical raindrops calculated by the XFDTD software and GMM algorithm were found consistent and matched well. Thus, XFDTD software can be used to calculate the RCS of non-spherical raindrops considering multiple scattering effects. The RCS values calculated by the simple addition method were smaller than those calculated by the XFDTD software and the GMM algorithm. The maximum relative difference given by the XFDTD software was 89.649% and the minimum relative difference was 43.701%, which means that multiple scattering effects of an ensemble of particles is an important factor affecting the retrieval of microphysical parameters of particles from radar data.

4. RCS Calculation of Raindrops

4.1 RCS Comparison Between Spherical and Non-Spherical Particles of Equivalent Volume

In this paper, the complex refractive index and complex permittivity of raindrops given in Table 2 were chosen when the RCS of raindrops was calculated. In XFDTD software, plane waves of S, C, X and Ku bands were set as excitation sources. The incident direction of the plane wave is Theta=180°, Phi=0°, and the polarization direction is E_x (that is, the electromagnetic wave is incident in the positive direction of the Z axis, and the polarization direction is along the X axis).

Using equations (1) and (2), we calculated the axial ratios of flat ellipsoid raindrops whose spherical equivalents have the following diameters: 3000 μm, 5000 μm, 7000 μm, and 9000 μm . The results are presented in Table 5. The placement of equivalent flat ellipsoid model in the coordinate simulated using the XFDTD software is shown in Figure 5.

RCS of spherical raindrops with diameters of 3000 μm, 5000 μm, 7000 μm, and 9000 μm, and of their equivalent flat ellipsoidal particles both calculated by XFDTD software, are shown in Table 6. It can be seen from Table 6 that the RCS of the spherical raindrops calculated by the XFDTD software is smaller than the RCS of the equivalent flat ellipsoidal raindrops. The observed maximum and minimum differences were 11.586 dB and 0.296 dB, respectively. These results suggest that the non-spherical shape of raindrops in actual precipitation swarms should be considered.

Table 5. Equivalent flat ellipsoid parameters

Diameter of equivalent spherical raindrop (μm)	Long axis of flat ellipsoid a (μm)	Short axis of flat ellipsoid c (μm)	Axis ratio
3000	1590	1340	0.84
5000	2790	2010	0.72
7000	4160	2480	0.60
9000	5780	2730	0.47

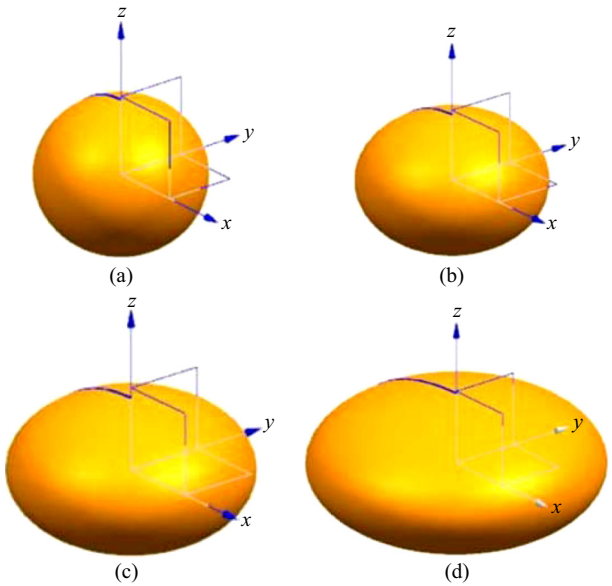

Figure 5. Schematic diagram of four equivalent flat ellipsoid particles in the XFDTD software. (a–d) The equivalent sphere diameter is 3000 μm, 5000 μm, 7000 μm, and 9000 μm respectively.

4.2 RCS Comparison Between Single Scattering and Multiple Scattering by Non-Spherical Raindrops

The spherical raindrops with diameters of 3000 μm, 5000 μm, 7000 μm, and 9000 μm shown in Figure 5 were replaced by the equivalent flat ellipsoids presented in Table 5 with the same arrangement; the resulting concrete distribution is shown in Figure 6. RCS values of the non-spherical raindrops given in Figure 6 were calculated by the XFDTD software. The computed results are tabulated in Table 7. Table 7 reveals that large average relative differences exist between RCS values computed by the simple addition method and those calculated by XFDTD. Among the differ-

Table 6. Comparison of the RCS of spherical raindrops and of their equivalent ellipsoidal oval raindrops computed by XFDTD (unit: dBm^2)

Diameter (μm)	Shape	S	C	X	Ku
3000	Sphere	−87.232	−76.795	−68.110	−63.079
	Flat ellipsoidal	−86.007	−75.800	−67.063	−62.783
5000	Sphere	−74.473	−66.757	−55.926	−50.802
	Flat ellipsoidal	−72.457	−63.662	−44.340	−41.961
7000	Sphere	−66.747	−45.429	−44.447	−42.195
	Flat ellipsoidal	−62.863	−44.870	−37.680	−40.641
9000	Sphere	−63.865	−42.117	−37.465	−40.726
	Flat ellipsoidal	−55.707	−39.882	−36.841	−35.319

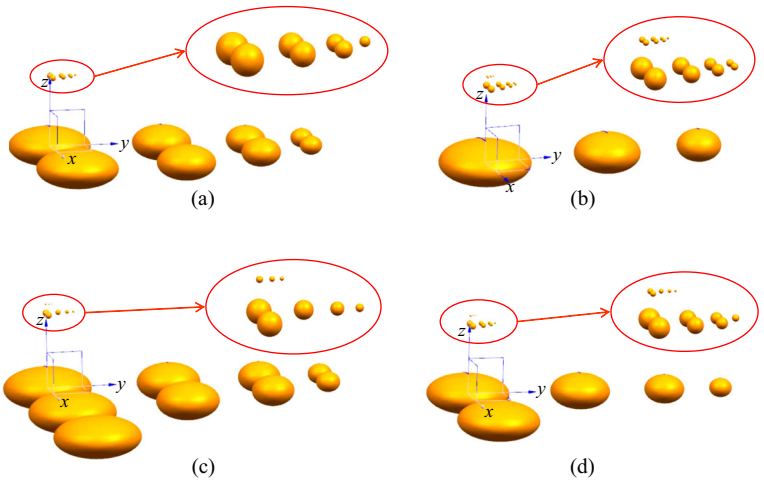

Figure 6. Non-spherical particle swarms in the XFDTD software layout diagram. (a-d) Non-spherical raindrops Arrangement 1 in Gamma, JD, JT and MP size distribution, respectively.

Table 7. RCS values for non-spherical raindrops using XFDTD, compared to RCS values computed by the simple addition method (unit: dBm^2)

Size distribution	Method	S	C	X	Ku
Gamma	XFDTD	–45.220	–32.734	–25.108	–22.340
	Simple addition method	–51.853	–35.661	–30.814	–30.513
JD	XFDTD	–52.040	–38.123	–31.379	–28.531
	Simple addition method	–54.866	–38.672	–33.826	–33.528
JT	XFDTD	–42.449	–29.736	–23.953	–20.710
	Simple addition method	–50.355	–34.268	–30.000	–29.208
MP	XFDTD	–46.935	–33.354	–28.032	–25.087
	Simple addition method	–54.863	–38.671	–33.824	–33.523

ent raindrop size distributions, RCS calculations for the JD distribution showed the smallest average relative difference 42.785% between computation methods. The largest average relative difference between RCS values calculated by the different methods was between those for the MP size distribution 78.451%. Among the various radar bands, the minimum relative difference in RCS values was 49.072%, for C band incident electromagnetic waves. The Ku band exhibited the largest relative difference, 81.164%, between RCS values calculated by different bands.

5. Error Analysis of the Relative Importance of Considering Multiple Scattering Effects, Non-Spherical Raindrop Shapes, and Different Particle Arrangements

In conventional meteorological radar data analysis, the meteorological target echo values are calculated using the radar meteorological equation based on Rayleigh scattering of small spherical particles. In order to assess the importance of considering multiple scattering and non-spherical raindrop shapes in radar parameters retrieval, the RCS values calculated by the XFDTD and simple addition methods (given in Table 4 and Table 7, respectively) are next compared to those calculated by the Rayleigh scattering formula. The comparison also includes the effects of different particle arrangements. The RCS formula of Rayleigh scattering is

$$\sigma = \frac{\pi^5}{\lambda^4}\left|\frac{m^2-1}{m^2+2}\right|\int_0^{D_{\max}} N(D)D^6\mathrm{d}D, \tag{7}$$

where λ is the wavelength of the incident electromagnetic wave, m is the refractive index of the raindrop particles, D is the equivalent diameter, $D_{\max}$ is the maximum particle equivalent diameter, and $N(D)$ is the distribution of particles. Results of the various RCS computations applied to the model in Figure 7 are shown in Table 8.

The particle arrangement in Figure 6 is called Arrangement 1 in this paper; its transformed version, shown in Figure 7, is termed Arrangement 2. The computed RCS values of the particles in Figure 7 are given in Table 8. Discussion of data summarized in Table 8.

(1) **Multiple Scattering vs. Rayleigh**. RCS values computed by XFDTD software that considers multiple scattering differ significantly from values given by the Rayleigh formula. The relative errors at the four size distributions considered in our analysis are 169.522%, 37.176%, 216.455%, and 63.428%, respectively.

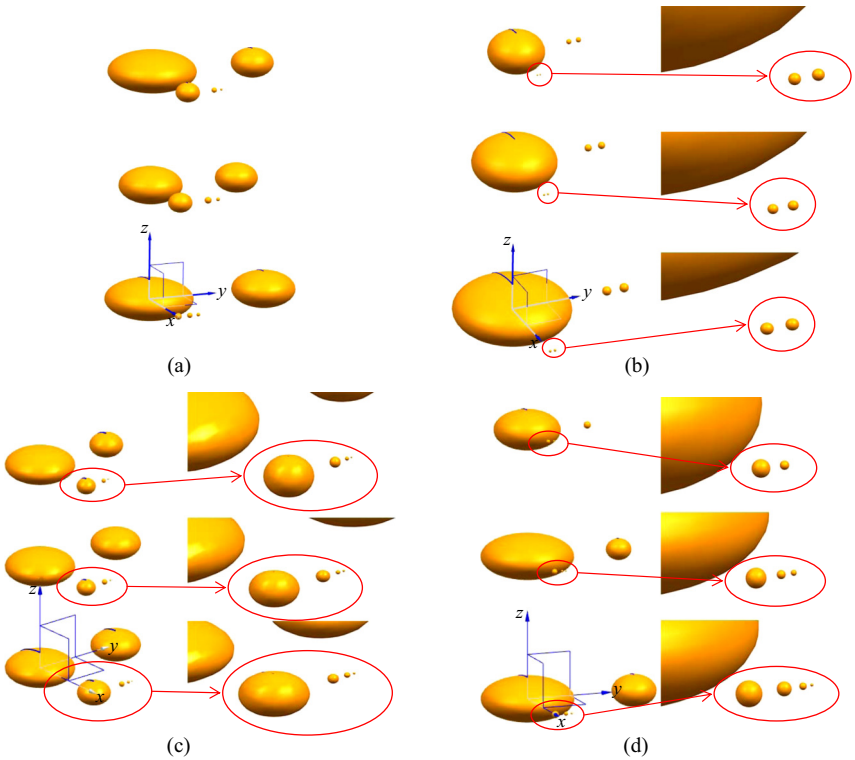

Figure 7. Layout diagram of non-spherical particles in the XFDTD software. (a–d) Non-spherical raindrops in Arrangement 2 at Gamma, JD, JT, MP size distribution, respectively.

Table 8. The influence of multiple scattering, non-spherical particles and particle arrangements on RCS (unit: dBm^2)

Size distribution	Method	Shape	Arrangement	Multiple scattering	S	C	X	Ku
Gamma	Rayleigh scattering formula	Sphere	—	No	−55.372	−44.128	−34.419	−27.967
	XFDTD	Sphere	1	Yes	−49.383	−35.009	−28.121	−24.532
	Simple addition method	Non–sphere	—	No	−51.853	−35.661	−30.814	−30.513
	XFDTD	Non–sphere	1	Yes	−45.220	−32.734	−25.108	−22.340
	XFDTD	Non–sphere	2	Yes	−62.526	−37.234	−26.149	−29.496
JD	Rayleigh scattering formula	Sphere	—	No	−58.387	−47.143	−37.434	−30.982
	XFDTD	Sphere	1	Yes	−58.114	−38.132	−34.042	−30.858
	Simple addition method	Non–sphere	—	No	−54.866	−38.672	−33.826	−33.528
	XFDTD	Non–sphere	1	Yes	−52.040	−38.123	−31.379	−28.531
	XFDTD	Non–sphere	2	Yes	−58.349	−41.888	−33.700	−42.926
JT	Rayleigh scattering formula	Sphere	—	No	−53.913	−42.669	−32.960	−26.508
	XFDTD	Sphere	1	Yes	−48.784	−29.819	−25.906	−22.812
	Simple addition method	Non–sphere	—	No	−50.355	−34.268	−30.000	−29.208
	XFDTD	Non–sphere	1	Yes	−42.449	−29.736	−23.953	−20.710
	XFDTD	Non–sphere	2	Yes	−65.298	−46.487	−29.083	−31.810
MP	Rayleigh scattering formula	Sphere	—	No	−55.833	−44.590	−34.880	−28.428
	XFDTD	Sphere	1	Yes	−53.651	−33.909	−30.826	−27.691
	Simple addition method	Non–sphere	—	No	−54.863	−38.671	−33.824	−33.523
	XFDTD	Non–sphere	1	Yes	−46.935	−33.354	−28.032	−25.087
	XFDTD	Non–sphere	2	Yes	−61.676	−48.72	−31.563	−29.586

(2) **Inclusion of Non-Spherical Effects vs. Rayleigh**. Comparing results of the Rayleigh formula with RCS values computed by considering non-spherical effects, the relative errors at the four size distributions are smaller than those associated with multiple scattering: 0.213%, 0.171%, 7.683%, and 44.514%, respectively.

(3) When the comparison is between the Rayleigh model and models that consider both multiple scattering effects and effects caused by non-spherical particles in the swarms, the RCS differences at the four size distributions are larger; the relative errors are 220.673%, 129.320%, 387.240%, and 186.613%, respectively.

(4) **Particle Arrangement Effects**. After changing the arrangement of particles at four size distributions in the case of multiple scattering effect and non-spherical effect, the RCS values of Arrangement 2 are smaller than those of Arrangement 1, and the relative errors are 60.558%, 76.263%, 85.941%, and 64.852%, respectively.

These results verify that consideration of multiple scattering, non-spherical particle shapes, and particle arrangements definitely affect computation of RCS values. Of the variables we have considered, multiple scattering effects appear to be the most important; the influence of non-spherical particle shapes is the least important.

6. Optimization of Simulation Time

When the RCS values of particles were calculated by XFDTD for this study, in our traditional method the spacing of particles in the swarms had to be subdivided into a large number of very small cells, all of the same size, in order to ensure the accuracy of the calculations for even the smallest particles. This required a long computation time. Taking Figure 6a as an example, the concrete particles can be as shown in Figure 8, the space of particles in the white box should be divided into cells with a side length of 150 μm, to accommodate the smallest particles. In this case, the calculation time needed for the XFDTD software was 42.117 hours.

In this paper, we divided the total particle swarm space into different regions by particle sizes, and then the regions were divided into different cell sizes appropriate to the particles in each region. As shown in Figure 9, the particle swarm spaces were divided into 5 regions, namely the white squares in the figure. The first four regions contain, respectively, two 9000 μm particles, two 7000 μm particles, two 5000 μm particles, and two 3000 μm particles; the fifth contains two 900 μm particles, two 700 μm particles, two 500 μm particles, and one 300 μm particle. We divided the 5 regions into cell sizes of 450 μm, 350 μm, 250 μm, 150 μm and 45 μm respectively; these cell sizes all meet the minimum computational accuracy of particles in their regions by our experiments. The calculation time of XFDTD was thus reduced to 31.483 hours.

Therefore, we shortened the calculation time of XFDTD, at the same time preserving the accuracy of the results. This provides a valuable technique that improves the usefulness of XFDTD in such calculations.

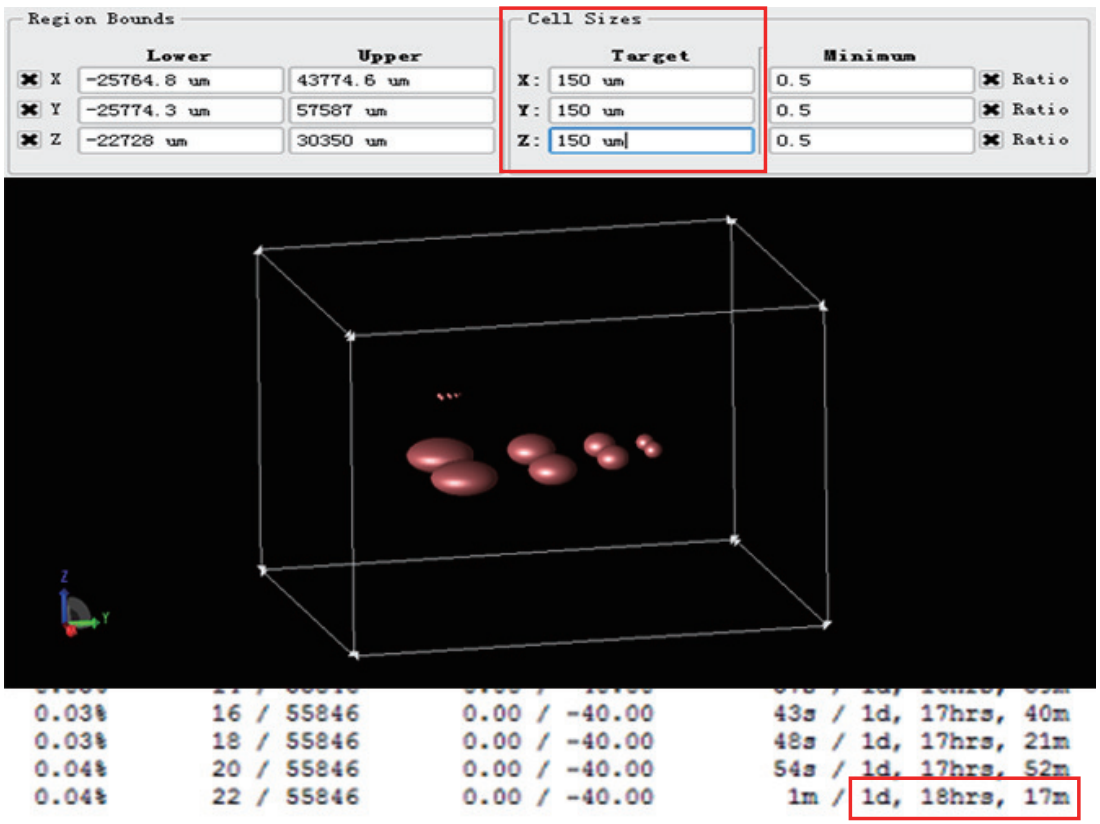

Figure 8. Cell size and calculation time for the space of particles.

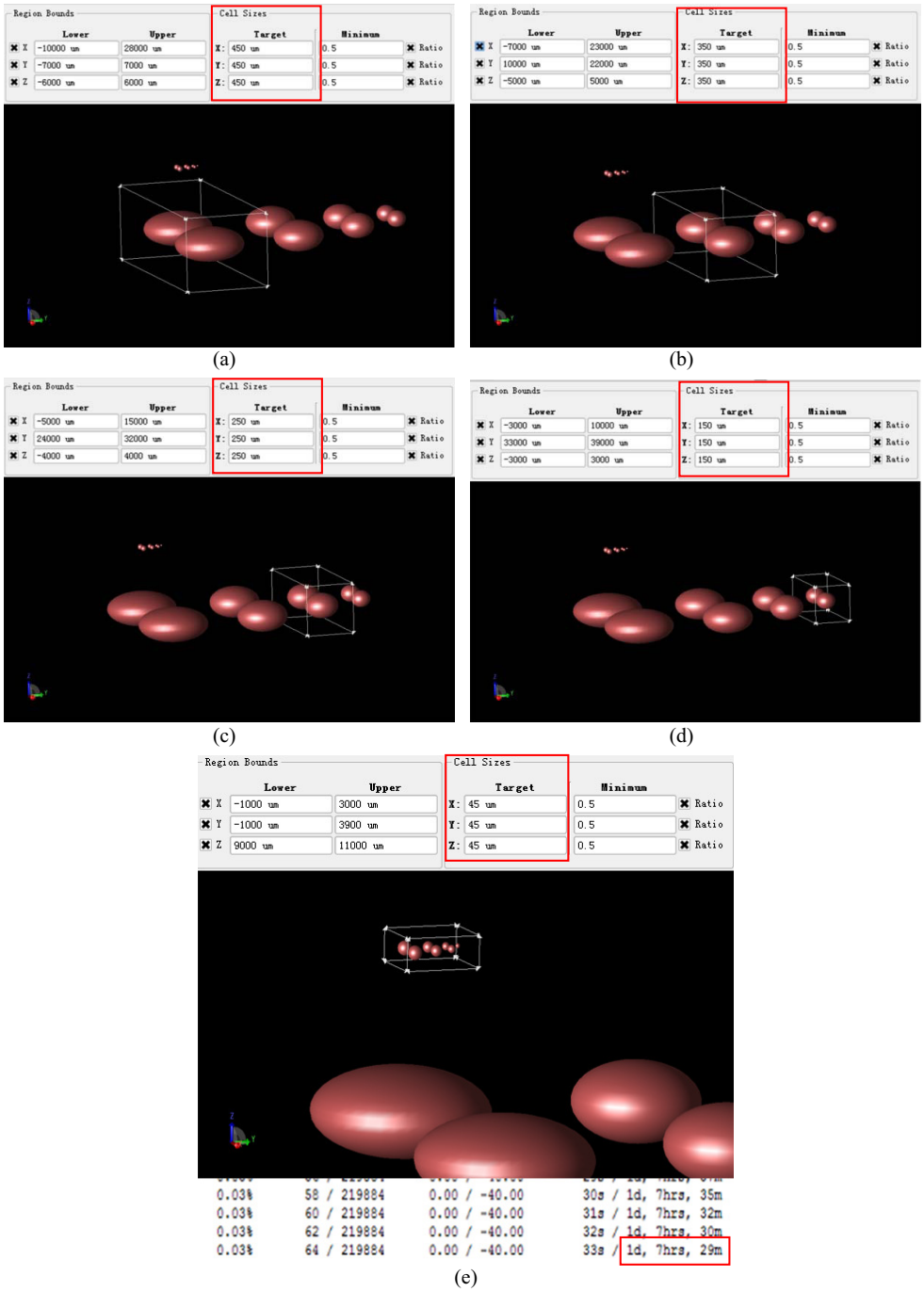

Figure 9. Surrounded regions and calculation time for the space of particles. (a–d) Cell size in regions 1, 2, 3 and 4, respectively. (e) Cell size in regions 5 and calculation time for the space of particles.

7. Conclusions

RCS values of the four spherical and non-spherical raindrops with Gamma, JD, JT, MP size distributions were calculated at S, C, X and Ku bands using XFDTD software and the simple addition method. The influence on RCS values of including considerations of multiple scattering and non-spherical particle shapes were analyzed. The results showed that : (1) For the same model, RCS values considering multiple scattering computed by the XFDTD software are larger than those calculated by the simple addition method; (2) For the spherical raindrop models, the maximum and minimum relative difference of the two methods is 89.649% and 43.701% respectively; (3) For the non-spherical raindrop models, the maximum and minimum relative difference of the two methods is 85.868% and 11.875%, respectively.

Comparing XFDTD multiple scattering calculations with Rayleigh formula results (which are commonly used in meteorological radar studies), we find the multiple scattering RCS values to be larger, differing from Rayleigh RCS results, for the same four size distributions, by relative errors of 169.522%, 37.176%, 216.455%, and 63.428%, respectively.

Comparing RCS values computed considering non-spherical effects with Rayleigh formula computations, we find that consideration of non-spherical effects yields values at the above four size distributions that are smaller than those given by Rayleigh; the relative errors are 0.213%, 0.171%, 7.683%, and 44.514%, respectively.

When Rayleigh formula RCS values are compared to RCS values that consider not only multiple scattering effects but also effects of non-spherical shapes in the particle swarms, at the above four size distributions, we find that the latter RCS values are larger; the relative errors are 220.673%, 129.320%, 387.240%, and 186.613%, respectively.

Two arrangements of particles at the four size distributions were used to assess the consequences of considering multiple scattering and non-spherical particle shapes. The RCS values computed for Arrangement 2 are smaller than those computed using Arrangement 1, and the relative errors are 60.558%, 76.263%, 85.941%, 64.852%, respectively.

We conclude that multiple scattering effects, the influence of non-spherical particle shapes, and the specific arrangement of particles in swarms all appear to affect RCS value computations. Among these considerations, the influence of the multiple scattering effect is the largest, and the influence of non-spherical shapes is the smallest.

We recommend that multiple scattering effects be considered in practical meteorological detection. In this paper, we have also suggested ways to optimize simulation time when using XFDTD software.

Acknowledgments

This work was supported by the Natural Science Foundation of Jiangsu Province (Grant No. BK20170945); the National Natural Science Foundation of China (Grant Nos. 41675029; 41275004; 61372066; 41571348); National Key Laboratory of Disaster Weather, China Academy of Meteorological Sciences (2016LASW-B12); the Key Laboratory for Aerosol-Cloud-Precipitation of CMA-NUIST (KDW1703); the Startup Foundation for Introducing Talent of Nanjing University of Information Science and Technology (2016r028); Earth Science Virtual Simulation Experiment Teaching Course Construction Project of Nanjing University of Information Science and Technology (XNFZ2017C02). We sincerely thank Dr. K. R. Kumar for his assistance and efforts in correcting the work to improve its scientific content.

References

Atlas, D., Kerker, M., and Hitschfeld, W. (1953). Scattering and attenuation by non-spherical atmospheric particles. *J. Atmos. Terr. Phys.*, *3*(2), 108–119. https://doi.org/10.1016/0021-9169(53)90093-2

Atlas, D., Srivastava, R. C., and Sekhon, R. S. (1973). Doppler radar characteristics of precipitation at vertical incidence. *Rev. Geophys.*, *11*(1), 1–35. https://doi.org/10.1029/RG011i001p00001

Bai, J. J., Li, Y., and Zhao, B. (2017). Directional light scattering from individual Au nanocup. *Opt. Commun.*, *387*, 208–213. https://doi.org/10.1016/j.optcom.2016.11.062

Bruscaglioni, P., Ismaelli, A. and Zaccanti, G. (1995). Monte-Carlo calculations of LIDAR returns: Procedure and results. *Appl. Phys. B*, *60*(4), 325–329. https://doi.org/10.1007/BF01082266

Chen, M. X., Yu, X. D., Tan, X. G., and Wang, Y. C. (2004). A brief review on the development of nowcasting for convective storms. *J. Appl. Meteor. Sci.* (*in Chinese*), *15*(6), 754–766.

Draine, B. T., and Flatau, P. J. (1994). Discrete-dipole approximation for scattering calculations. *J. Opt. Soc. Am. A*, *11*(4), 1491–1499. https://doi.org/10.1364/JOSAA.11.001491

Eremin, J. A., Orlov, N. V., and Rozenberg, V. I. (1995). Multiple electromagnetic scattering by a linear array of electrified raindrops. *J. Atmos. Terr. Phys.*, *57*(3), 311–319. https://doi.org/10.1016/0021-9169(94)P4361-2

Konoshonkin, A. V., Kustova, N. V. Shishko, V. A., and Borovoi, A. G. (2016). The technique for solving the problem of light backscattering by ice crystals of cirrus clouds by the physical optics method for a Lidar with zenith scanning. *Atmos. Oceanic Opt.*, *29*(3), 252–262. https://doi.org/10.1134/S1024856016030088

Kunkel, K. E., and Weinman, J. A. (1976). Monte Carlo analysis of multiply scattered Lidar returns. *J. Atmos. Sci.*, *33*(9), 1772–1781. https://doi.org/10.1175/1520-0469(1976)033<1772:MCAOMS>2.0.CO;2

Li, S. H., Sun, X. M, Wang, H. H., and Lei, C. X. (2014). Study on electromagnetic wave scattering by raindrops. *J. Light Scattering* (*in Chinese*), *26*(1), 1–7.

Li, Y. Y., Sun, D. S., Wang, Z. Z., Shen, F. H., Zhou, X. L., and Dong, J. J. (2008). Study of clouds multiple-scattering influence on Lidar measurement. *Laser Technol.* (*in Chinese*), *32*(6), 611–613.

Liu C., Bi, L., Lee Panetta, R., Yang, P., and Yurkin, M. A. (2012a). Comparison between the pseudo-spectral time domain method and the discrete dipole approximation for light scattering simulations. *Opt. Express*, *20*(15), 16763–16776. https://doi.org/10.1364/OE.20.016763

Liu, C., Lee Panetta, R., and Yang, P. (2012b). Application of the pseudo-spectral time domain method to compute particle single-scattering properties for size parameters up to 200. *J. Quant. Spectrosc. Radiat. Transfer*, *113*(13), 1728–1740. https://doi.org/10.1016/j.jqsrt.2012.04.021

Liu, L. P., and Xu, B. X. (1991). A study of scattering and attenuation properties of model hail with different phase at 5.6 cm wavelength. *Plateau Meteor.* (*in Chinese*), *10*(1), 26–33.

Liu, X. C., Gao, T. C., Qin, J., and Liu, L. (2010). Effects analysis of rainfall on microwave transmission characteristics. *Acta Phys. Sin.* (*in Chinese*), *59*(3), 2156–2162.

Liu, X. C., Gao, T. C., Liu, L., and Hu, S. (2013). Advances in microphysical features and measurement techniques of raindrops. *Adv. Earth Sci.* (*in Chinese*), *28*(11), 1217–1226.

Loiko, V. A., Konkolovich, A. V., Zyryanov, V. Y., and Miskevich, A. A. (2017). Small-angle light scattering symmetry breaking in polymer-dispersed liquid crystal films with inhomogeneous electrically controlled interface anchoring. *J. Exp. Theor. Phys.*, *124*(3), 388–405. https://doi.org/10.1134/S1063776117020133

Mason, B. J. (1979). *The Physics of Clouds* (*in Chinese*) (pp. 343–345). The Institute of Atmospheric Physics, Chinese Academy of Sciences, trans. Beijing: Science Press.

Mätzler, C. (2002). Drop-size distributions and Mie computations for rain. Research Report No.16. Switzerland: Institute of Applied Physics, University of Bern.

Mishchenko, M. I. (1993). Light scattering by size-shape distributions of randomly oriented axially symmetric particles of a size comparable to a wavelength. *Appl. Opt.*, *32*(24), 4652–4666. https://doi.org/10.1364/AO.32.004652

Mishchenko, M. I., Travis, L. D. and Mackowski, D. W. (1996). *T*-matrix computations of light scattering by nonspherical particles: A review. *J. Quant. Spectrosc. Radiant. Transfer*, *55*(5), 535–575. https://doi.org/10.1016/0022-4073(96)00002-7

Mishchenko, M. I., Hovenier, J. W., and Travis, L. D. (2000). *Light Scattering by Nonspherical Particles: Theory, Measurements, and Applications*. New York: Academic Press.

Mooradian, G. C., Geller, M., Levine, P. H., Stotts, L. B., and Stephens, D. H. (1980). Over-the-horizon optical propagation in a maritime environment. *Appl.*

Opt., *19*(1), 11–30. https://doi.org/10.1364/AO.19.000011

Platt, C. M. R., and Dilley, A. C. (1984). Determination of the cirrus particle single-scattering phase function from Lidar and solar radiometric data. *Appl. Opt.*, *23*(3), 380–386. https://doi.org/10.1364/AO.23.000380

Pruppacher, H. R., and Beard, K. V. (1970). A wind tunnel investigation of the internal circulation and shape of water drops falling at terminal velocity in air. *Quart. J. Roy. Meteor. Soc.*, *96*(408), 247–256. https://doi.org/10.1002/(ISSN)1477-870X

Pruppacher, H. R., and Pitter, R. L. (1971). A semi-empirical determination of the shape of cloud and rain drops. *J. Atmos. Sci.*, *28*(1), 86–94. https://doi.org/10.1175/1520-0469(1971)028<0086:ASEDOT>2.0.CO;2

Seliga, T. A., and Bringi, V. N. (1978). Differential reflectivity and differential phase shift: Applications in radar meteorology. *Radio Sci.*, *13*(2), 271–275. https://doi.org/10.1029/RS013i002p00271

Spinhirne, J. D. (1982). Lidar clear atmosphere multiple scattering dependence on receiver range. *Appl. Opt.*, *21*(14), 2467–2468. https://doi.org/10.1364/AO.21.002467

Taflove, A. (1998). *Advances in Computational Electrodynamics*. Boston, MA: Artech House.

Taflove, A., and Hagness, S. C. (2000). *Computational Electrodynamics*. Boston, MA: Artech House.

Wang, G. L., Liu, L. P., and Ruan, Z. (2007). Application of Doppler radar data to nowcasting of heavy rainfall. *J. Appl. Meteor. Sci.* (*in Chinese*), *18*(3), 388–395.

Wang, J. H., Ge, J. X., Wei, M., and Yu, W. W. (2013). Influence of scattering properties due to complex refractive index of ice. In *Proceedings of the 3rd International Conference on Information Science and Technology* (pp. 997–999). Yangzhou, Jiangsu, China: IEEE. https://doi.org/10.1109/ICIST.2013.6747704

Wang, J. H., Ge, J. X., and Wei, M. (2014). Theoretical study on single-scattering properties of ice particles of different orientation at 94 GHz. *Prog. Electromagn. Res. M*, *36*, 39–46. https://doi.org/10.2528/PIERM14033106

Wang, J. H., Ge, J. X., Zhang, Q. L., Li, X. C., Wei, M., Yang, Z. X., and Liu, Y. A. (2016a). Radar cross-section measurements of ice particles using vector network analyzer. *AIP Adv.*, *6*(9), 095310. https://doi.org/10.1063/1.4963080

Wang, J. H., Ge, J. X., Zhu, X., Wei, M., Yang, Z. X., and Li, J. Q. (2016b). Effect of orientation and air content of ice particles on radar reflectivity factor. *J. Infrared Millim. Waves* (*in Chinese*), *35*(1), 78–86.

Wang, J. H., Ge, J. X., Wei, M., Gu, S. S., and Yang, Z. X. (2016c). Study of the relationship between IWC and Z for nonspherical ice particles at millimeter wavelength. *J. Trop. Meteor.*, *22*(S1), 78–88.

Wang, K., Do, K. D., and Cui, L. (2017). Underwater active electrosense: A scattering formulation and its application. *IEEE Trans. Rob.*, *33*(5), 1233–1241. https://doi.org/10.1109/TRO.2017.2694829

Wang, Z. H. (2002). Study on backscattering experiment and DDA calculation of spherical cone ellipsoid. *Journal of Nanjing Institute of Meteorology*, *25*(3), 307–313.

Wang, Z. H., Xu, X. Y., Wang, Q. A., and Chao, Z. M. (2003). Comparison between the lab observations and DDA computations on the backscattering features of sphere-cone-oblate ice particles. *J. Quant. Spectrosc. Radiat. Transfer*, *77*(4), 455–462. https://doi.org/10.1016/S0022-4073(02)00165-6

Xiong, X. L., Li, M., Jiang, L. H., Feng, S., and Zhuang, Z. B. (2014). The study of the Lidar ratio retrieval method with multiple scattering cirrus cloud. *J. Optoelectron. Laser* (*in Chinese*), *25*(6), 1158–1164.

Wu, J. X., Wei, M., Zhou, J., and Wang, J. H. (2012). Effects of temperature and orientation on 3.2 mm radar backscattering from ice crystals. In *Proceedings of the 5th International Conference on Advanced Computational Intelligence* (pp. 742–746). Nanjing, China: IEEE. https://doi.org/10.1109/ICACI.2012.6463266

Xu, L. S., Chen, H. B., Ding, J. L., and Xia, Z. Y. (2014). An overview of the advances in computational studies on light scattering by nonspherical particles. *Adv. Earth Sci.* (*in Chinese*), *29*(8), 903–912.

Xu, X. Y. (2002). Scattering of microwaves by non-spherical raindrops and hails (*in Chinese*). Nanjing: Nanjing University of Information Engineering, [Master's thesis].

Xu, Y. L. (1995). Electromagnetic scattering by an aggregate of spheres. *Appl. Opt.*, *34*(21), 4573–4588. https://doi.org/10.1364/AO.34.004573

Xu, Y. L., and Gustafson, B. Å. S. (1997). Experimental and theoretical results of light scattering by aggregates of spheres. *Appl. Opt.*, *36*(30), 8026–8030. https://doi.org/10.1364/AO.36.008026

Yang, P., and Liou, K. N., (1996). Finite-difference time domain method for light scattering by small ice crystals in three-dimensional space. *J. Opt. Soc. Am. A*, *13*(10), 2072–2085. https://doi.org/10.1364/JOSAA.13.002072

Yee, S. (1996). Numerical solution of initial boundary value problems involving Maxwell's equations in isotropic media. *IEEE Trans. Antennas Propag.*, *14*(3), 302–307.

Zhang, P. C., and Wang, Z. H. (1995). *Analysis of Atmospheric Microwave Remote Sensing* (*in Chinese*). Beijing: Meteorological Press,16–19.

Zhong, L. Z., Liu, L. P., and Ge, R. S. (2009). Characteristics about the millimeter-wavelength radar and its status and prospect in and abroad. *Adv. Earth Sci.* (*in Chinese*), *24*(4), 383–391.